Journal of Cleaner Production 515 (2025) 145773

Contents lists available at ScienceDirect

Journal of Cleaner Production

journal homepage: www.elsevier.com/locate/jclepro

Selective extraction of Mg^{2+} from chrysotile asbestos tailings via ammonium sulfate roasting and water leaching: Process optimization and mechanistic insights

Lingyan Chu [a,b], Hongjuan Sun [a,b,*], Tongjiang Peng [a,b], Haichen Lu [a,b], Maoting Li [a,b], Yiqin Zhang [a,b], Liming Luo [a,b]

[a] Key Laboratory of Solid Waste Treatment and Resource Reuse, Ministry of Education, Southwest University of Science and Technology, Mianyang, 621010, Sichuan, China

[b] Institute of Mineral Materials and Applications, Southwest University of Science and Technology, Mianyang, 621010, Sichuan, China

ARTICLE INFO

Keywords:
Chrysotile asbestos tailings
Ammonium sulfate roasting
Selective extraction
Magnesium sulfate

ABSTRACT

Chrysotile asbestos tailings, while posing significant environmental risks due to their biotoxicity, represent an underutilized magnesium reservoir. This study uses ammonium sulfate roasting-water leaching strategy for selective Mg^{2+} extraction from Chrysotile asbestos tailings with the inhibition of impurity ion leaching, simultaneously addressing hazardous waste management and Mg^{2+} selective recovery. The findings disclosed that the leaching rate of Mg^{2+} was 84.18 % at a molar ratio of sulfate to magnesium oxide in chrysotile asbestos tailings of 1.0, roasting temperature of 650 °C, roasting time of 90 min, liquid-to-solid ratio of 8 mL/g, and leaching temperature of 30 °C. Meanwhile, the leaching rates of Fe^{2+}/Fe^{3+}, Al^{3+}, Cr^{3+}, Ni^{2+}, and Ca^{2+} are found to be 0.04 %, 0.24 %, 0.09 %, 5.37 %, and 53.61 %, respectively; the purity of Mg^{2+} in the filtrate is measured as high as 98.87 %. Mechanistic insights show that ammonium sulfate reacts with metal ions in chrysotile asbestos tailings to form soluble sulfates at high temperatures. Because of the difference in thermal stability of different metal ions sulfate, $MgSO_4$ dissolves during water leaching, while Fe^{2+}, Fe^{3+}, Al^{3+}, Cr^{3+}, and Ni^{2+} remain in the residue due to their sulfate convert to insoluble oxides conversion. Life cycle assessment identifies the roasting process as the primary contributor to carbon emissions, highlighting energy optimization as a critical target for sustainable and scale-up.

1. Introduction

Magnesium compounds are important inorganic materials whose industrial value increases with purity (Li et al., 2025). In recent years, driven by high-end industries such as aerospace, automotive, electronics and new energy, the global market demand for high-purity magnesium compounds has shown a rapid growth trend (Tian et al., 2024). Forecasts indicate a compound annual growth rate (CAGR) of 4.9 % in the global magnesium market, with the market expanding from 1.1 million metric tons (Mt) in 2020 to 1.6 Mt by 2027 (Tan and Ramakrishna, 2021). This growing demand is in stark contrast to the depletion of traditional magnesium sources such as magnesite. In this context, the development of efficient magnesium recovery technologies based on secondary resources (such as industrial solid waste) has become an urgent need to restructure the sustainable magnesium supply chain. Chrysotile asbestos tailings, a solid waste abundant in Mg^{2+}, are a promising but underutilized source of Mg^{2+}.

Chrysotile asbestos tailings, a by-product of chrysotile exploiting and processing, predominantly contain 40 %~50 % SiO_2 and 35 %~45 % MgO, along with trace amounts of Fe_3O_4, Al_2O_3, and CaO (Hui et al., 2021; Tan et al., 2021). Chrysotile asbestos mining regions are mainly situated in Canada, the United States, China, and Italy, where over several decades extensive mining and processing have produced hundreds of millions of tons of chrysotile asbestos tailings (Cavallo, 2020; Dong et al., 2015). It is concerning that these asbestos tailings are often open pit without covering. (Lévesque et al., 2020). The residual asbestos fibers in the tailings are prone to dispersion by wind, which can lead to respiratory diseases in surrounding communities, such as lung cancer

* Corresponding author. Key Laboratory of Ministry of Education for Solid Waste Treatment and Resource Recycle, Southwest University of Science and Technology, Mianyang, 621010, Sichuan, China.
E-mail address: sunhongjuan@swust.edu.cn (H. Sun).

https://doi.org/10.1016/j.jclepro.2025.145773
Received 22 January 2025; Received in revised form 10 May 2025; Accepted 20 May 2025
Available online 22 May 2025

and malignant mesothelioma (Thives et al., 2022). Furthermore, the storage of asbestos tailings also occupies land resources, resulting in the waste of mineral resources (Kabombo et al., 2021; Li et al., 2024; Zheng et al., 2020).

Therefore, the selective extraction of Mg^{2+} from chrysotile asbestos tailings may address high purity magnesium resource shortages and reduce the environmental consequences of solid waste accumulation. Chrysotile, the primary Mg^{2+}-bearing mineral in these tailings, is a 1:1 layered magnesium silicate. Key Mg^{2+}extraction methods include acid leaching and roasting. Acid leaching employs inorganic or organic acids to decompose the chrysotile structure (El-Sayed et al., 2023), dissolving Mg^{2+} into the acidic solution. However, this process co-dissolves impurities like Fe^{3+}, Fe^{2+}, and Al^{3+} (Kaya and Topkaya, 2011; Lu et al., 2022, 2023). Removing these impurities can lead to Mg^{2+} loss and generate hard-to-use residues (Alexander et al., 2007). Furthermore, acid leaching poses difficulties including equipment corrosion due to the acidic solution and substantial alkali consumption during neutralization (Baigenzhenov et al., 2015). Roasting, often combined with acid leaching, uses high-temperature treatment to destroy the chrysotile structure, reducing acid consumption during leaching (Liu et al., 2022; Raschman et al., 2013). Furthermore, the researchers also explored roasting with additive as an alternative method to lower the decomposition temperature of chrysotile and enhance Mg^{2+} extraction. Common promoters include ammonium sulfate and ammonium bisulfate. Bei Song et al. demonstrated that calcination of asbestos tailings with ammonium sulfate could achieve Mg^{2+} extraction rates of up to 68.56 % (Song et al., 2015). However, all above methods fail to address the issues of impurity co-dissolution and residue generation during purification (Sanna et al., 2013). These challenges highlight the need for further optimization of extraction processes to improve efficiency and environmental sustainability.

The ammonium sulfate ($(NH_4)_2SO_4$) roasting process has lately garnered interest owing to its benefits of low energy usage, reduced equipment corrosion, and good selectivity (Liu et al., 2024). This process converts target metal ions into water-soluble sulfates while transforming impurities into insoluble compounds (Liu et al., 2023; Tagawa, 1984), enabling selective metal leaching (Ju et al., 2023a, 2023b, 2024). The selectivity of $(NH_4)_2SO_4$ roasting and water leaching has been extensively demonstrated in various minerals. Jinrong Ju et al. employed the $(NH_4)_2SO_4$ roasting and water leaching method on pyrolusite, achieving a manganese leaching rate of 96.15 % and an iron leaching rate of merely 1.45 %, with residual iron existing as hematite (Ju et al., 2023c). Yanchun Li et al. employed sulfate roasting and water leaching to extract zinc from zinc leaching residues, achieving a zinc leaching rate of 92.63 % while maintaining an iron leaching rate of 2.04 % (Li et al., 2015). However, systematic studies on the selective extraction of Mg^{2+} from chrysotile asbestos tailings using this method are still lacking. Additionally, the potential environmental impact of this process has not been assessed.

This work is based on that chrysotile tailings are rich in Mg^{2+} and have a small amount of metal ions such as Fe^{3+}, Al^{3+} and Cr^{3+}. The Mg^{2+} was selectively extracted by $(NH_4)_2SO_4$ roasting followed by water leaching to separate Mg^{2+} from Fe^{3+} and other impurities. The effects of roasting conditions and leaching conditions on the leaching rates of Mg^{2+} and other impurity metal ion was carefully examined to identify the optimal process parameters for the selective extraction of Mg^{2+}. The alteration in phase composition and microstructure during roasting and water leaching were analyzed to clarify the process of selective Mg^{2+} extraction from chrysotile asbestos tailings via the $(NH_4)_2SO_4$ roasting-water leaching method. Furthermore, a life cycle assessment was conducted to evaluate the environmental impact of each process stage, with optimization suggestions provided to enhance sustainability. This work not only offers a novel technical approach for Mg^{2+} extraction from chrysotile asbestos tailings but also holds promise for the processing of other Mg-rich minerals, contributing to the development of more sustainable and efficient magnesium recovery technologies.

2. Materials and methods

2.1. Materials and reagents

The chrysotile asbestos tailings utilized in this study were procured from the Hongliugou chrysotile asbestos mine located in Aksay, Gansu Province, China. The tailings were initially subjected to crushing and grinding, followed by drying in an oven at 105 °C for 24 h to eliminate free and adsorbed water within the samples. Subsequently, the dried samples were labeled as "CAT". The median particle diameter of the CAT sample was 8.41 μm (Fig. 1a). The phase composition of the CAT sample was quantitatively analyzed using X-ray diffraction (XRD) (Fig. 1b) and the calcium fluoride external standard method (Fig. 1c). The results indicate that the CAT samples primarily consist of 61.6 % chrysotile, 10.5 % amorphous phase, 10.4 % chlorite, along with minor amounts of quartz, talc, and magnetite. Given the limitations of XRD in distinguishing serpentine polymorphs, Raman spectroscopy was used. It identified chrysotile and lizardite in CAT samples (Fig. 1d) (Liu et al., 2023). However, in the subsequent analyses, further differentiation of these two polymorphs was not carried out due to the focus being on the overall serpentine reaction. The chemical composition mainly consists of 41.33 % SiO_2, 41.59 % MgO, and a small amount of Fe_2O_3, Al_2O_3, and other components (Table 1).

The experiment utilized analytical grade chemical reagents, including $(NH_4)_2SO_4$ and EDTA-2Na, procured from Chengdu Chemical Reagent Co.

2.2. Experimental procedures

2.2.1. Roasting with $(NH_4)_2SO_4$ additive

The $(NH_4)_2SO_4$ and 2 g of the CAT sample were mixed at a predetermined molar ratio and thoroughly blended in an agate mortar to ensure a fine and uniform mixture. The mixture was transferred into a crucible and placed into a muffle furnace, where it was heated to the desired temperature at a rate of 10 °C/min and then held at that temperature for a certain period. After the roasting was completed, the calcined samples were collected and labeled as B-T-M-t, where "B" indicates the calcined sample, "T" denotes the roasting temperature (°C), "M" represents the molar ratio of $(NH_4)_2SO_4$ to MgO in the asbestos tailings, and "t" denotes the time of roasting (min).

2.2.2. Water leaching

The calcined samples were transferred into a conical flask containing deionized water and leached on a constant-temperature shaker for 1 h. After leaching, the resulting suspension was filtered with filter paper with an aperture of 20 μm and a Brinell funnel with a diameter of 9 cm, and the residue was washed with deionized water until neutral. The resulting leached residue was dried in an oven at 105 °C for 24 h, then stored in a sealed plastic bag and labeled as S-T-M-t, where "S" indicates the leached residue sample. The filtrate was collected, sealed in a conical flask, and labeled as FL-T-M-t, where "FL" denotes the filtrate (Fig. 2).

2.3. Characterization

The chemical composition of chrysotile asbestos tailings was analyzed using an Axios X-ray fluorescence (XRF) spectrometer. The sample preparation was conducted by pressing the sample into pellets. Test conditions were as follows: ceramic X-ray tube (Rh target), maximum power of 2.4 kW.

Thermal analysis was performed using a STA449F5 thermal analyzer under the following conditions: heating rate of 10 °C/min, temperature range from room temperature to 1000 °C, and air atmosphere. The reference material used was α-Al_2O_3.

The concentration of SO_2 gas during the roasting process was measured using a Korn SO_2 gas analyzer, with continuous reading testing mode.

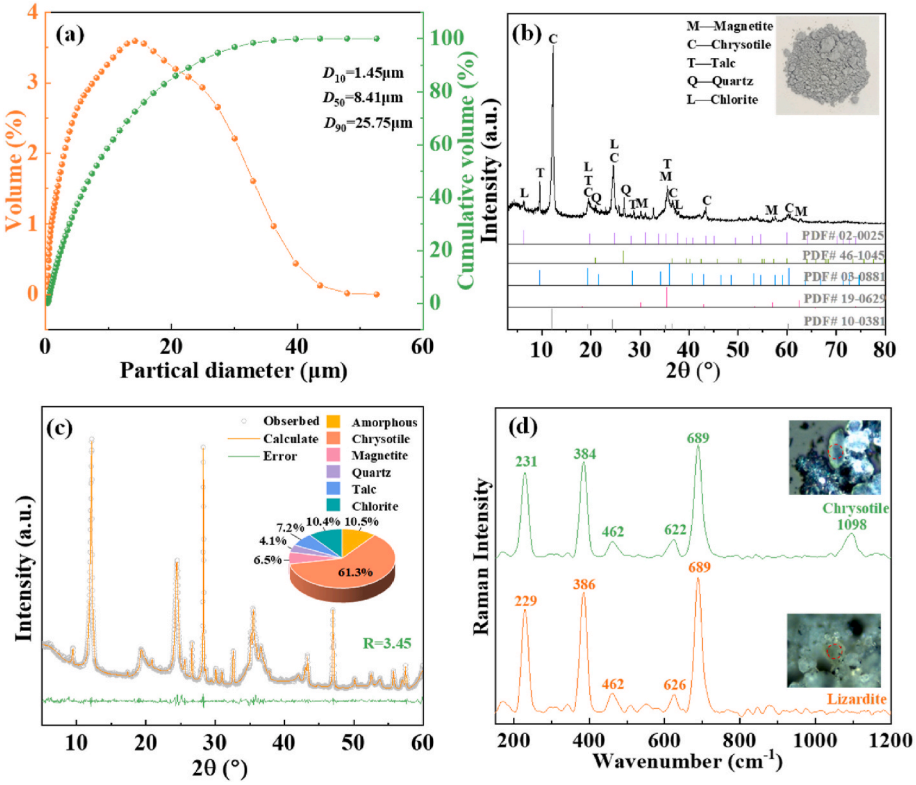

Fig. 1. Size distribution (a), XRD pattern (b), phase composition (c) and Raman spectrum (d) of CAT sample.

Table 1
The chemical compositions of CAT sample (wt.%).

Component	SiO_2	MgO	Fe_2O_3	Al_2O_3	CaO	Cr_2O_3	NiO	TiO	MnO_2	K_2O	P_2O_5	LOI
Content	41.33	41.59	3.09	1.20	0.47	0.42	0.21	0.08	0.06	0.03	0.03	12.74

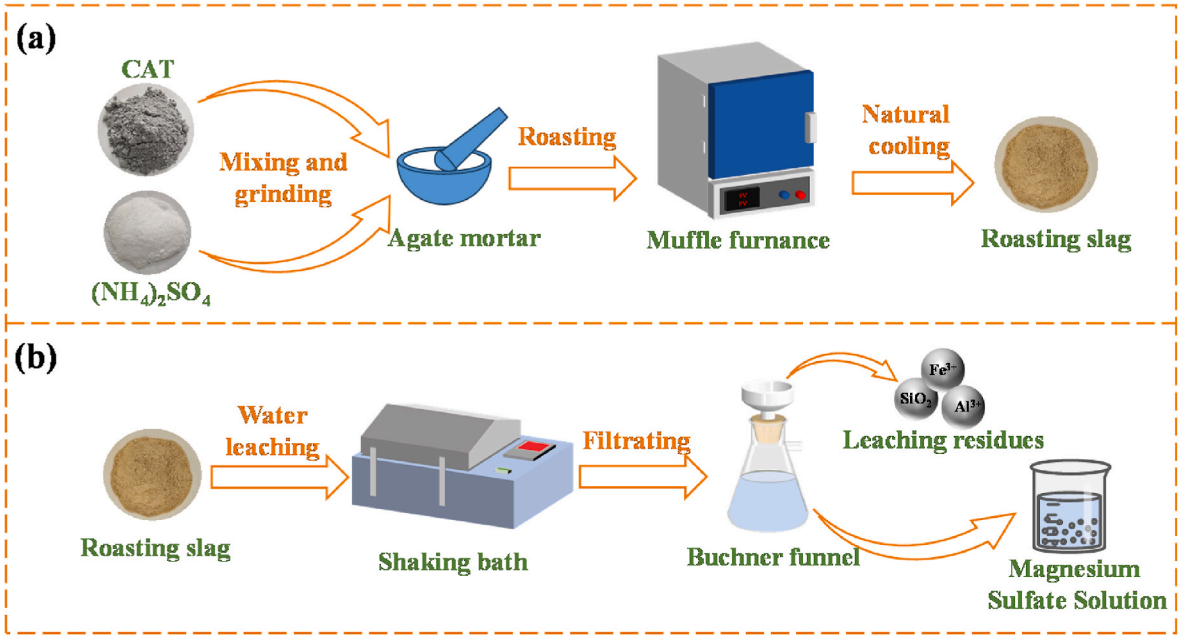

Fig. 2. Experimental flow diagram for roasting with $(NH_4)_2SO_4$ additive (a) and water leaching (b).

The phase composition and structure of the samples were analyzed using an X'pert MPD Pro X-ray diffractometer. Test conditions: Cu target, tube voltage of 40 kV, tube current of 40 mA, emission slit (DS): (1/2) °, scatter slit (SS): 0.04 rad, and receiving slit (AAS): 5.5 mm; continuous scanning mode.

The microscopic morphology of the samples was observed using a Sigma300 field-emission scanning electron microscope (SEM). The testing conditions were as follows: working voltage of 10 kV, energy resolution >127 eV, and magnification range from × 50 to × 1,000,000. Energy dispersive spectroscopy (EDS) was performed with an X-MAXN20 energy spectrometer. The test conditions were: working voltage of 15 kV, energy resolution >127 eV, and magnification range from × 50 to × 1,000,000.

The concentrations of Al^{3+}, Ca^{2+}, Cr^{3+}, and Ni^{2+} ions in the filtrate were determined using an Agilent 5110 plasma spectrometer, with a wavelength range of 166~847 nm and a cooling temperature of < -40 °C.

The concentrations of Fe^{2+}/Fe^{3+} in the filtrate were measured using an Evolution 300 UV–Vis spectrophotometer. Mg^{2+} concentrations in the filtrate were determined by EDTA standard titration.

The leaching rate (α) of each ion was calculated using the following formula:

$$\alpha = CV/M \times 100\ \% \quad (1)$$

Where C is concentration of the specific ion in the filtrate (mg/L), V is total volume of the filtrate (L), M is total mass of the specific element in the chrysotile asbestos tailings (mg).

The purity (P) of Mg^{2+} in the solution was calculated using the following formula:

$$P = C_{Mg}/C_{Tol} \times 100\ \% \quad (2)$$

Where C_{Mg} is concentration of Mg^{2+} in the filtrate (mg/L), C_{Tol} concentration of all metal ions in the filtrate (mg/L).

3. Results and discussion

3.1. Thermodynamic analysis

The thermal decomposition of $(NH_4)_2SO_4$ occurs in three stages: Initially, $(NH_4)_2SO_4$ decomposes into NH_4HSO_4 between 246 °C and 328 °C (Eq. (1)), which then decomposes into $(NH_4)_2S_2O_7$ between 328 °C and 346 °C (Eq. (2)). Finally, $(NH_4)_2S_2O_7$ decomposes into NH_3, SO_2, and other gases between 346 °C and 430 °C (Eq. (3)) (Zhou et al., 2013). Given the presence of multiple intermediate products, the thermodynamic calculations focus solely on the reactions of $(NH_4)_2SO_4$ and NH_4HSO_4 with CAT sample.

$$(NH_4)_2SO_4 \rightarrow NH_4HSO_4 + NH_3 \quad (1)$$

$$2NH_4HSO_4 \rightarrow (NH_4)_2S_2O_7 + H_2O \quad (2)$$

$$3(NH_4)_2S_2O_7 \rightarrow 2NH_3 + 6SO_2 + 2N_2 + 9H_2O \quad (3)$$

During the roasting of $(NH_4)_2SO_4$ and CAT, potential reactions involve chrysotile reacting with $(NH_4)_2SO_4$ or its decomposition product NH_4HSO_4 to form $MgSO_4$ (Eq. (4) and (5)). Magnetite reacts with $(NH_4)_2SO_4$ or NH_4HSO_4 to form $Fe_2(SO_4)_3$ and $FeSO_4$ (Eq. (6) and (7)). Thermodynamic calculations using HSC Chemistry 6 software revealed that chrysotile can spontaneously react with $(NH_4)_2SO_4$ or NH_4HSO_4 to form $MgSO_4$ above 245 °C and 48 °C, respectively (Fig. 3a). Magnetite can spontaneously react with $(NH_4)_2SO_4$ or NH_4HSO_4 to form $Fe_2(SO_4)_3$ and $FeSO_4$ above 319 °C and 77 °C, respectively. However, since the decomposition of $(NH_4)_2SO_4$ to NH_4HSO_4 occurs above 230 °C, the reaction temperatures of chrysotile and magnetite with NH_4HSO_4 must exceed 230 °C.

$$Mg_3Si_2O_5(OH)_4 + 3(NH_4)_2SO_4 \rightarrow 3MgSO_4 + 2SiO_2 + 6NH_3 + 5H_2O \quad (4)$$

$$Mg_3Si_2O_5(OH)_4 + 3NH_4HSO_4 \rightarrow 3MgSO_4 + 2SiO_2 + 3NH_3 + 5H_2O \quad (5)$$

$$Fe_3O_4 + 4(NH_4)_2SO_4 \rightarrow Fe_2(SO_4)_3 + FeSO_4 + 8NH_3 + 4H_2O \quad (6)$$

$$Fe_3O_4 + 4NH_4HSO_4 \rightarrow Fe_2(SO_4)_3 + FeSO_4 + 4NH_3 + 4H_2O \quad (7)$$

The high-temperature decomposition reactions of the sulfate of the

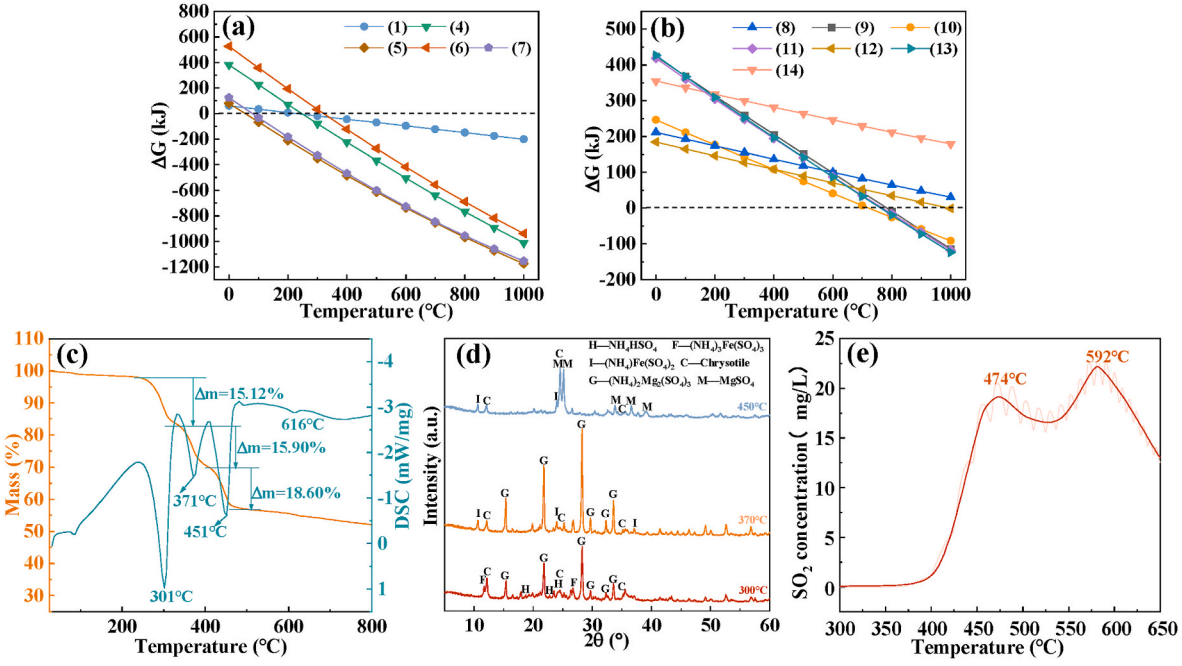

Fig. 3. Variation of Gibbs free energies with temperature for Eq. (1) to Eq. (7) (a) and Eq. (8) to Eq. (14) (b); TG–DSC curve (c), XRD pattern (d) and SO_2 release concentrations at different roasting temperatures (e) of a mixture of $(NH_4)_2SO_4$ and CAT samples with a molar ratio of $(NH_4)_2SO_4$ to MgO of 1:1.

main metal ions in CAT are shown in Eqs. (8)–(14), with corresponding ΔG-T diagrams in Fig. 3b. The theoretical decomposition temperatures of $Fe_2(SO_4)_3$, $FeSO_4$, $Al_2(SO_4)_3$, $NiSO_4$, and $Cr_2(SO_4)_3$ are 778 °C, 710 °C, 769 °C, 782 °C, and 758 °C, respectively, while the decomposition temperature of $MgSO_4$ is considerably above 1000 °C. Given that $MgSO_4$ is highly soluble in water, whereas Fe_2O_3, Al_2O_3, NiO, and Cr_2O_3 are insoluble, Mg^{2+} can be effectively separated from Fe^{2+}, Fe^{3+}, Al^{3+}, Cr^{3+}, and Ni^{2+} through water leaching. This forms the basis for the approach discussed in this study.

$$MgSO_4 \rightarrow MgO + SO_3 \quad (8)$$

$$Fe_2(SO_4)_3 \rightarrow Fe_2O_3 + 3SO_3 \quad (9)$$

$$2FeSO_4 \rightarrow Fe_2O_3 + SO_3(g) + SO_2 \quad (10)$$

$$Al_2(SO_4)_3 \rightarrow Al_2O_3 + 3SO_3 \quad (11)$$

$$NiSO_4 \rightarrow NiO + SO_3 \quad (12)$$

$$Cr_2(SO_4)_3 \rightarrow Cr_2O_3 + 3SO_3 \quad (13)$$

$$CaSO_4 \rightarrow CaO + SO_3 \quad (14)$$

While Gibbs free energy calculations confirm the thermodynamic feasibility of chrysotile and magnetite sulfation reactions (Eqs. (4)–(7)), practical implementation is governed by kinetic constraints and process parameters. To elucidate the reaction pathways, the $(NH_4)_2SO_4$ and CAT were thoroughly mixed in a 1:1 M ratio of $(NH_4)_2SO_4$ to MgO for thermal analysis and phase analysis. The TG-DSC profile (Fig. 3c) reveals four distinct weight loss events between 25 and 800 °C, each accompanied by an endothermic dip. The initial weight loss, observed between 246 °C and 336 °C with an approximate weight loss of 15.12 %. XRD analysis (Fig. 3d) indicates that at this temperature, $(NH_4)_2SO_4$ decomposes into NH_4HSO_4, with the diffraction peaks of chrysotile weakening, which is consistent with the thermodynamic results of Eq. (1). Concurrently, $(NH_4)_3Fe(SO_4)_3$ and $(NH_4)_2Mg_2(SO_4)_3$ are formed. This suggests that the mass loss in this stage is primarily attributed to the decomposition of chrysotile and $(NH_4)_2SO_4$. The second weight loss stage occurs between 336 °C and 411 °C, with a loss rate of approximately 15.90 %. XRD analysis shows that the diffraction peaks of chrysotile continue to

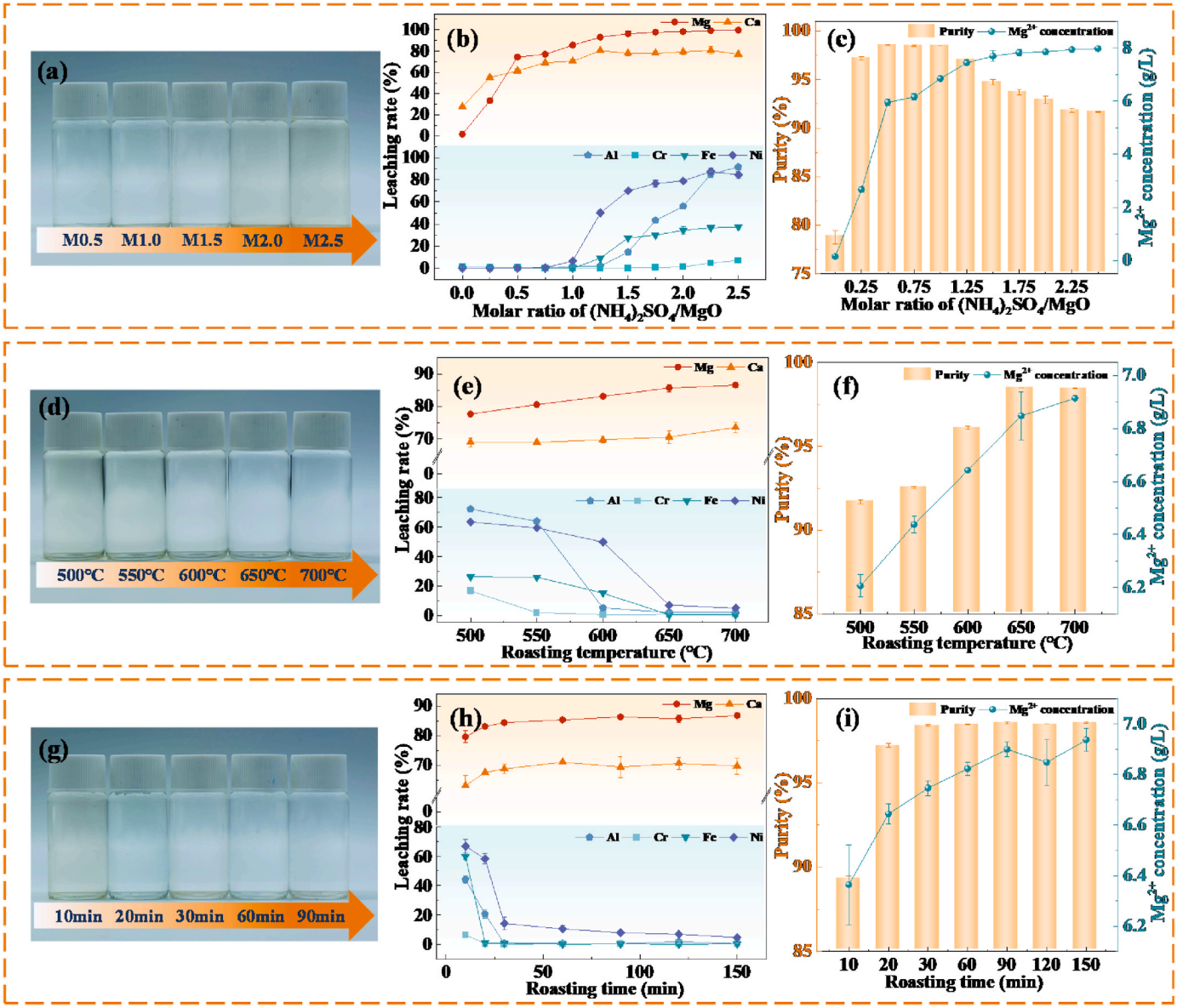

Fig. 4. Photographs of water-leaching solutions from roasting slag at different $(NH_4)_2SO_4$ additions (a), roasting temperatures (d) and roasting times (g); Leaching rates of metal ions from roasting slag at different $(NH_4)_2SO_4$ additions (b), roasting temperatures (e) and roasting times (h); Concentration and purity of Mg^{2+} in the filtrate at different $(NH_4)_2SO_4$ additions (c), roasting temperatures (f) and roasting times (i).

weaken, while the characteristic diffraction peaks of $(NH_4)_2Mg_2(SO_4)_3$ are enhanced. This indicates that chrysotile and NH_4HSO_4 continue to decompose and react. In addition, $(NH_4)_3Fe(SO_4)_3$ is transformed into $(NH_4)Fe(SO_4)_2$. Therefore, the mass loss in this stage is mainly due to the further decomposition of NH_4HSO_4, chrysotile, and $(NH_4)_3Fe(SO_4)_3$. The third weight loss phase takes place between 411 °C and 511 °C, with an approximate loss of 18.60 %. XRD analysis reveals that the diffraction peaks of chrysotile further weaken, and $(NH_4)_2Mg_2(SO_4)_3$ decomposes into $MgSO_4$. This indicates that the mass loss in this stage is primarily due to the further decomposition of chrysotile and $(NH_4)_2Mg_2(SO_4)_3$. The fourth endothermic dip occurs at 616 °C with a minor weight loss. Based on the thermodynamic data of Eq. (8) to Eq. (14), this stage is likely associated with the decomposition of metal sulfates such as $Fe_2(SO_4)_3$, $FeSO_4$, $Al_2(SO_4)_3$, $NiSO_4$, and $Cr_2(SO_4)_3$ (Andersen et al., 2021; Lacalamita et al., 2021).

To monitor the formation and decomposition of sulfates during the roasting process of the $(NH_4)_2SO_4$/CAT mixture, an SO_2 gas detector was used to track the release of SO_2. As illustrated in Fig. 3e, the results reveal two primary release temperatures for SO_2. The initial peak at 474 °C aligns with the temperature at which SO_2 is released from the decomposition of $(NH_4)_2SO_4$ (Zhou et al., 2013). Meanwhile, the second peak at 592 °C corresponds to the decomposition of metal sulfates, including those of Fe^{2+}, Fe^{3+}, Al^{3+}, Cr^{3+}, and Ni^{2+}. This is consistent with the thermodynamic decomposition temperatures of these metal sulfates as shown in Fig. 3b.

3.2. Effects of $(NH_4)_2SO_4$ roasting process parameters on the selective leaching of Mg^{2+}

3.2.1. The impact of $(NH_4)_2SO_4$ addition

The leaching rates of various metal ions in the roasting slags were depicted in Fig. 4b as a function of $(NH_4)_2SO_4$ addition. The data show that the leaching rates of the metal ions are significantly influenced by the amount of $(NH_4)_2SO_4$. As the molar ratio of $(NH_4)_2SO_4$ to MgO in CAT increases from 0 to 0.5, the leaching rate of Mg^{2+} increases sharply from 1.93 % to 74.52 %. This is attributed to the enhanced interaction between Mg^{2+} in the CAT and $(NH_4)_2SO_4$, forming soluble $MgSO_4$ Li et al., 2018; Li et al., 2017).Further increasing the molar ratio to 1.5 leads to a slower increase in the leaching rate of Mg^{2+}, reaching 96.36 %. Beyond this point, further additional $(NH_4)_2SO_4$ yield minimal improvements in Mg^{2+} leaching. A similar trend is observed for Ca^{2+}, whose leaching rate also increases with higher $(NH_4)_2SO_4$ addition. In contrast, the leaching rates of Fe^{2+}/Fe^{3+} remain low and stable when the molar ratio between 0 and 1.0, as Fe^{2+}/Fe^{3+} primarily exist as insoluble hematite in the leach residues. However, as the molar ratio increases from 1.0 to 2.5, the leaching rate of Fe^{2+}/Fe^{3+} increase significantly, likely attributed to the excess $(NH_4)_2SO_4$ reacting with Fe^{2+}/Fe^{3+} to form soluble iron sulfate salts (Lente and Fábián, 2002). The leaching of Al^{3+}, Cr^{3+}, and Ni^{2+} is negligible when the molar ratio is below 1.0. When the molar ratio exceeds 1.0, these ions begin to leach significantly. Furthermore, the leaching of Fe^{2+}, Fe^{3+}, Al^{3+}, Cr^{3+}, and Ni^{2+} is negligible when the molar ratio is less than 1.0. When the molar ratio exceeds 1.0, these ions begin to leach significantly. At low $(NH_4)_2SO_4$ concentrations, $(NH_4)_2SO_4$ preferentially reacts with Mg^{2+} and Ca^{2+} to form soluble sulfates (Xiao et al., 2015). When the molar ratio exceeds 1.0, Fe^{2+}, Fe^{3+}, Al^{3+}, Cr^{3+}, and Ni^{2+} begin to leach significantly, and the filtrate color also changes from colorless to yellow (Fig. 4a). This is because excess $(NH_4)_2SO_4$ reacts with these ions to form sulfates, which are not complete to decompose during roasting and are easily dissolved during water leaching (Liu et al., 2012).

Fig. 4c shows the purity and Mg^{2+} concentration of the filtrate as a function of $(NH_4)_2SO_4$ addition. As the quantity of $(NH_4)_2SO_4$ increases, the purity of Mg^{2+} in the filtrate first rises and subsequently declines, because excess $(NH_4)_2SO_4$ increases the leaching rate of other metal ions. To ensure efficient selective separation of Mg^{2+} and maintain a high leaching rate, a molar ratio of 1.0 for $(NH_4)_2SO_4$ to MgO in CAT was optimal.

3.2.2. Influence of roasting temperature

Fig. 4e presents the leaching rates of various metal ions in the roasting slags as a function of roasting temperature. Roasting temperature significantly affects the leaching rates of metal ions from CAT. As the roasting temperature increases from 500 °C to 650 °C, leaching rate of Mg^{2+} rises from 77.73 % to 85.76 %, due to increased decomposition of chrysotile and its reaction with $(NH_4)_2SO_4$ to form soluble magnesium salts (Nduagu et al., 2014). However, when further increasing the roasting temperature to 700 °C, there is almost no change observed in the leaching rate of Mg^{2+}, likely because some chrysotile converts to refractory forsterite (Chen et al., 2021). Similarly, the leaching rate of Ca^{2+} gradually increases with roasting temperature. In contrast, the leaching rates of Fe^{2+}/Fe^{3+} decrease significantly as the temperature rises from 500 °C to 650 °C and remain low above 650 °C. This decrease, accompanied by a color change in the filtrate from colorless to yellow (Fig. 4d), is due to $(NH_4)_2SO_4$ reacting with Fe^{2+}/Fe^{3+} to form $Fe_2(SO_4)_3$, which then converts to insoluble hematite at higher temperatures(Wu et al., 2023). Correspondingly, the leaching rates of Al^{3+}, Cr^{3+}, and Ni^{2+} decrease with increasing roasting temperature, as they transform from sulfates to insoluble oxides(Zhao et al., 2024).

Fig. 4f shows the concentration and purity of Mg^{2+} in the leachate as a function of roasting temperature. As the roasting temperature increases, the concentration of Mg^{2+} in the leachate initially rises and then stabilizes, while the purity of Mg^{2+} increases and then slightly declines. This is because, higher temperatures enhance Mg^{2+} leaching but also promote Ca^{2+} leaching. Based on these trends, 650 °C was chosen as the optimal roasting temperature.

3.2.3. Influence of roasting time

Fig. 4h shows the leaching rates of various metal ions in the roasting slags as a function of roasting time. Mg^{2+} leaching rises sharply as roasting time extends from 10 to 30 min, due to enhanced interaction between Mg^{2+} and $(NH_4)_2SO_4$, producing soluble magnesium sulfate(Lv et al., 2019). Meanwhile, the leaching rates of Al^{3+}, Cr^{3+}, Ni^{2+}, and Fe^{2+}/Fe^{3+} drop significantly, and the filtrate color shifts from yellow to colorless (Fig. 4g), as prolonged roasting transforms their sulfates into insoluble oxides(Mu et al., 2018). When the roasting time is further extended from 30 min to 150 min, the leaching rate of Mg^{2+} increases slowly, while the leaching rates of Fe^{2+}/Fe^{3+}, Al^{3+}, Cr^{3+}, Ni^{2+}, and Ca^{2+} stay nearly constant.

Fig. 4i shows the concentration and purity of Mg^{2+} in the leachate as a function of roasting time. As roasting time increases, both the concentration and purity of Mg^{2+} in the leachate initially rise and then stabilize. This trend indicates that extended roasting time not only enhances the leaching rate of Mg^{2+} but also suppresses the leaching of Fe^{2+}/Fe^{3+}, Al^{3+}, Cr^{3+}, and Ni^{2+}. Considering the energy consumption, 90 min was determined as the optimal roasting time.

3.3. Effects of water leaching process conditions on the selective leaching of Mg^{2+}

3.3.1. Influence of leaching temperature

In addition to the roasting conditions, the selective leaching results of chrysotile residues are also significantly influenced by water leaching conditions. Fig. 5a illustrates the leaching rates of different metal ions in the roasting slags as a function of leaching temperature. All metal ion leaching rates increase with rising temperature, attributed to enhanced solubility at higher temperatures(Rashid et al., 2020). The purity of the leachate decreases as the leaching temperature increases (Fig. 5b). This is because the elevated temperature promotes the co-leaching of Mg^{2+} and impurities (such as Fe^{2+}, Fe^{3+}, and Ca^{2+}). Based on both leaching rates and changes in leachate purity, a leaching temperature of 30 °C was selected as the optimal condition.

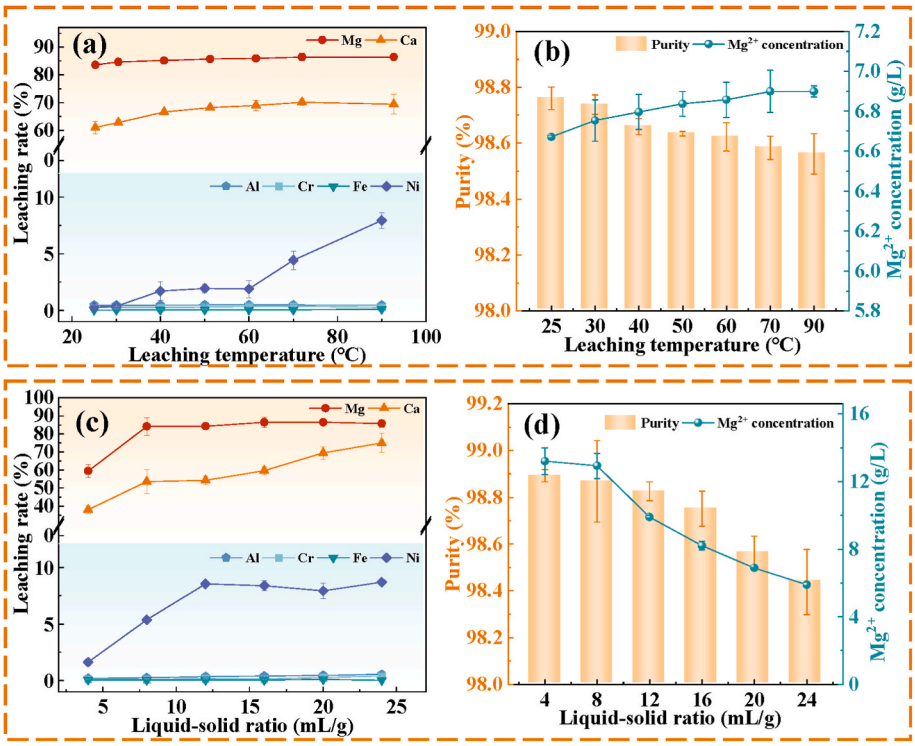

Fig. 5. Leaching rates of metal ions from roasting slag at different leaching temperatures (a) and liquid -to- solid ratio (c); Concentration and purity of Mg^{2+} in the filtrate at different leaching temperatures (b) and liquid -to- solid ratio (d).

3.3.2. *Influence of liquid-to-solid ratio in leaching*

Fig. 5c illustrates the leaching rates of different metal ions in the roasting slags relative to the liquid-to-solid ratio. As the liquid-to-solid ratio increases from 4 mL/g to 8 mL/g, the leaching rates of all metal ions markedly enhance. The rise is due to constraints in the reaction interface between the leaching solution and the calcined residue at a low liquid-to-solid ratio, leading to quick saturation of metal ion concentrations(Xu et al., 2021). The leachate purity increases as the liquid-to-solid ratio rises from 4 mL/g to 8 mL/g but slightly decreases with further increases (Fig. 5d). This is because while an increase in the liquid-to-solid ratio promotes the leaching of Mg^{2+}, it also enhances the leaching rates of impurity ions such as Fe^{2+}, Fe^{3+}, and Ca^{2+}. Considering all factors, a liquid-to-solid ratio of 8 mL/g was selected as optimal.

Based on single-factor experiments, the optimal process conditions were determined as follows: a molar ratio of $(NH_4)_2SO_4$ to MgO in CAT of 1.0, a roasting temperature of 650 °C, a roasting time of 90 min, a leaching temperature of 30 °C, and a liquid-to-solid ratio of 8 mL/g. Under these conditions, the leaching rate of Mg^{2+}, Fe^{2+}/Fe^{3+}, Al^{3+}, Cr^{3+}, Ni^{2+}, Ca^{2+} are respectively 84.18 %, 0.04 %, 0.24 %, 0.09 %, 5.37 %, 53.61 %, with a leachate purity of 98.87 %. While most impurity metal ions exhibited low leaching rates, the relatively high Ca^{2+} leaching rate significantly impacts the overall leachate purity.

3.4. *Mechanism of selective extraction of magnesium oxide via $(NH_4)_2SO_4$ roasting-leaching method*

3.4.1. *Phase composition of roasting slags and leaching residues*

Fig. 6a–f presents XRD analyses of roasting slags and leaching residues under various conditions, while Fig. 6g–i shows quantitative phase analyses of leaching residues using the calcium fluoride external standard method (3 % addition).

In Fig. 6a, the XRD spectrum of the roasting slags reveal the diffraction peaks of $MgSO_4$, indicating that $(NH_4)_2SO_4$ has reacted with chrysotile in the CAT sample to produce $MgSO_4$. As the $(NH_4)_2SO_4$ dosage increases, the intensity of the $MgSO_4$ diffraction peaks rises, while the full width at half maximum (FWHM) narrows, indicating enhanced crystallinity. Fig. 6b shows that the leaching residues contain insoluble substances, including chrysotile, hematite, talc, quartz, chlorite, and forsterite, while the diffraction peaks of $MgSO_4$ are absent. This confirms that $MgSO_4$ has dissolved into the solution through leaching. As the $(NH_4)_2SO_4$ dosage increases, the intensities and proportions of chrysotile, forsterite, and chlorite in the leaching residues decrease, while the content of amorphous phases rises (Fig. 6g). This reduction is attributed to the enhanced reactivity of $(NH_4)_2SO_4$ with minerals such as chrysotile, chlorite due to the increased dosage(Nduagu et al., 2014). Excess $(NH_4)_2SO_4$ reacts with Fe^{2+}/Fe^{3+} to form soluble sulfate(Li et al., 2017), reducing the hematite content in the leaching residues (Fig. 6g). This observation is consistent with the results in Fig. 4b, where the leaching rates of Fe^{2+}/Fe^{3+} and Al^{3+}increase as the amount of $(NH_4)_2SO_4$ to MgO in CAT exceeds a molar ratio of 1.0.

As shown in Fig. 6c, at a roasting temperature of 500 °C, the main phases in the roasting slags comprises chrysotile from the CAT sample and $MgSO_4$. With increasing temperature, the intensity of the $MgSO_4$ diffraction peaks is enhanced, while that of chrysotile diminishes. Fig. 6d illustrates that with the increase in roasting temperature, the intensity of the diffraction peaks of chrysotile in the leaching residues decrease, while that of hematite, chlorite and forsterite increase. Concurrently, the proportions of chlorite and chrysotile decrease, while the proportions of amorphous phases, forsterite, and hematite increase (Fig. h). This indicates that higher temperatures enhance the reactivity between $(NH_4)_2SO_4$ and chrysotile as well as chlorite, and promote the transformation of iron sulfate into hematite. However, excessively high temperatures can lead to the conversion of some chrysotile into forsterite (Song et al., 2013b).

Fig. 6e shows that at 10 min of roasting, the primary phases in the roasting slags are chrysotile and $MgSO_4$. As roasting time increases, the intensity of the diffraction peak of chrysotile weakens, while that of $MgSO_4$ increases. This indicates that prolonged roasting time promotes the reaction of $(NH_4)_2SO_4$ with chrysotile and the formation of $MgSO_4$. Fig. 6f shows that extended roasting times reduce chrysotile peak

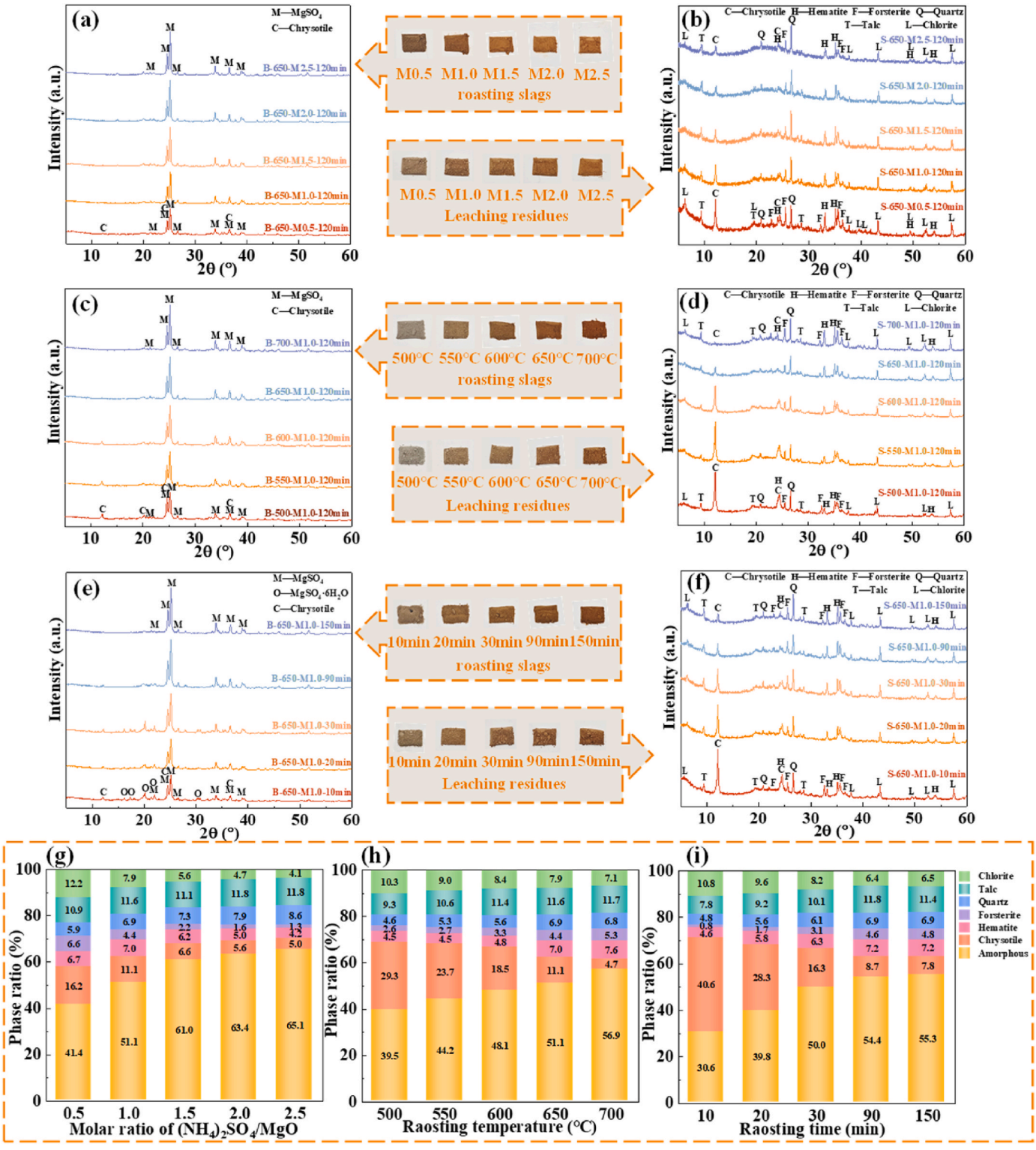

Fig. 6. XRD patterns of roasting slags at different $(NH_4)_2SO_4$ additions (a), roasting temperatures (c) and roasting times (e); XRD patterns of leaching residues at different $(NH_4)_2SO_4$ additions (b), roasting temperatures (d) and roasting times (f). Phase proportion of leaching residues at different $(NH_4)_2SO_4$ additions (g), roasting temperatures (h) and roasting times (i).

intensity in leaching residues and increase quartz peak intensity. The proportions of chlorite and chrysotile diminish in the leaching residues, while those of hematite and amorphous phases increase (Fig. 6i). This indicates that longer roasting times enhance the reaction between $(NH_4)_2SO_4$ and chrysotile as well as chlorite, while also facilitating the decomposition of iron sulfate into hematite (Deng et al., 2020; Li et al., 2022). Additionally, through the aforementioned analyses, it was found that under the conditions of this study, talc and quartz in the CAT sample hardly react.

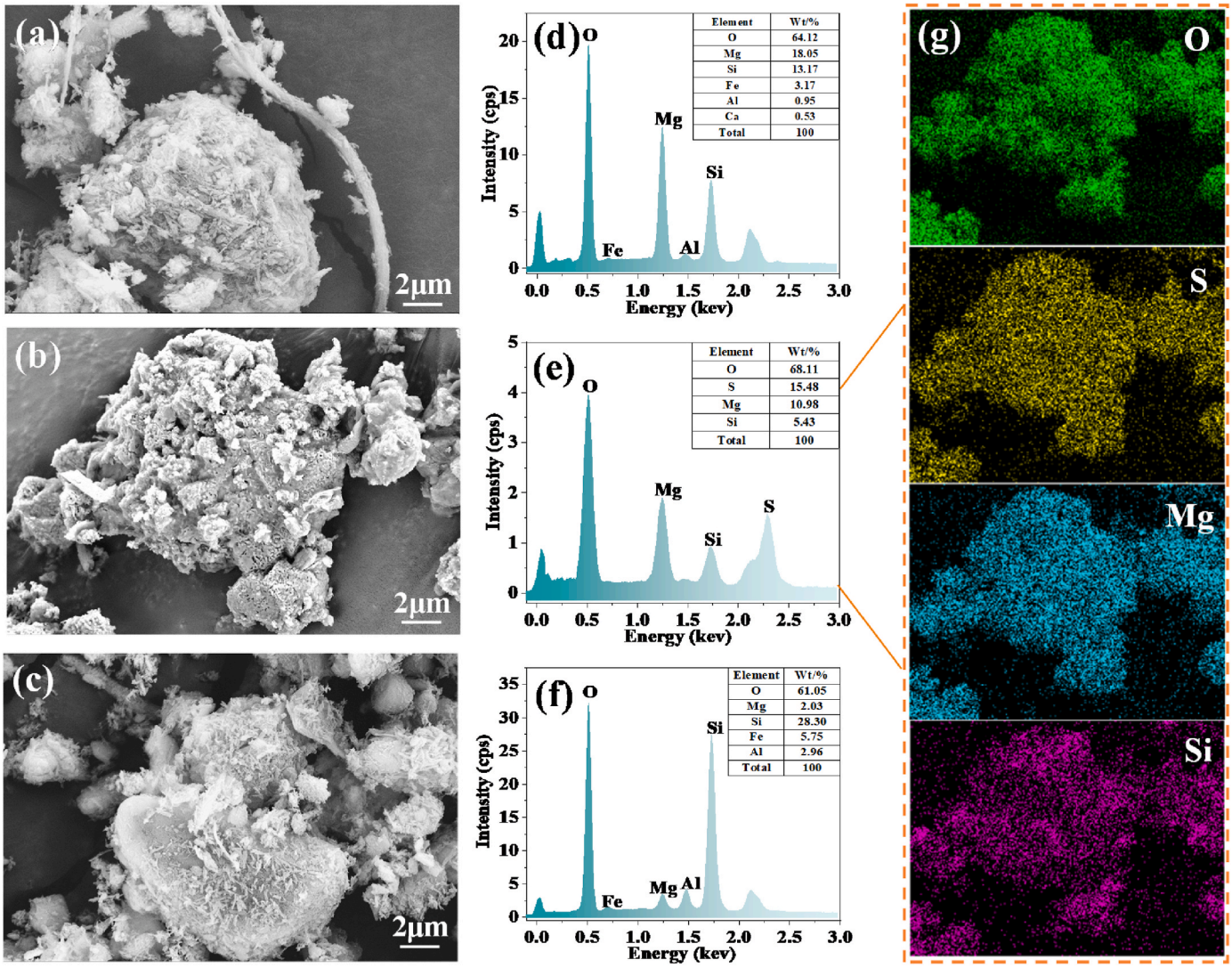

Fig. 7. Microscopic characteristics of CAT (a), roasting slag (b) and leaching residues (c) under optimal conditions; EDS of CAT (d), roasting slag (e) and roasting slags (f) under optimal conditions; Elemental mapping of O, S, Mg, and Si in the area of figure b (g).

3.4.2. Micromorphology of the roasting slags and leach residues from $(NH_4)_2SO_4$/CAT mixture

To elucidate the mechanism of selective extraction of Mg^{2+} from CAT through $(NH_4)_2SO_4$ roasting and subsequent water leaching, SEM-EDS analyses were performed on the original sample, roasting slags, and leaching residues, as seen in Fig. 7. The original CAT sample (Fig. 7a) consists of asbestos fibers and fine powder agglomerates. EDS analysis (Fig. 7d) shows high Mg content (18.05 %) and significant oxygen (64.12 %), consistent with chrysotile composition. After roasting with $(NH_4)_2SO_4$, the roasting slag (Fig. 7b) exhibits a molten and porous surface, indicating morphological changes due to chrysotile decomposition and $MgSO_4$ formation (Highfield et al., 2012). EDS analysis of the roasting slag (Fig. 7e) reveals increased sulfur (15.48 %) and magnesium (10.98 %), confirming $MgSO_4$ and other sulfate formation. EDS (Fig. 7g) shows a close spatial correlation between sulfur and magnesium, further confirming $MgSO_4$ formation during roasting. The leaching residues (Fig. 7c) show no fibers compared to the original CAT. This confirms chrysotile decomposition during roasting. EDS analysis of the leaching residues (Fig. 7f) shows a significant decrease in magnesium content (2.03 %), demonstrating effective $MgSO_4$ dissolution. Meanwhile, the increased Fe, Si, and Al contents in the residues indicate their retention as insoluble compounds like hematite and corundum.

Owing to the low concentrations of Fe, Al, Ni, and Cr in the CAT samples, XRD analysis and SEM imaging are unable to elucidate the transformations of these metal ions during the calcination process. Consequently, $(NH_4)_2SO_4$ was mixed with Fe_3O_4, Al_2O_3, NiO, and Cr_2O_3 reagents at a molar ratio of 1:1 and calcined at various temperatures for 60 min to investigate the transformations of Fe, Al, Ni, and Cr metal ions during the calcination process (Fig. 8). The results indicated that at a calcination temperature of 500 °C, Fe_3O_4 primarily transformed into $Fe_2(SO_4)_3$. As the temperature increased to 650 °C, the diffraction peaks of $Fe_2(SO_4)_3$ gradually weakened and ultimately disappeared, leading to complete transformation into hematite (Fe_2O_3). At 500 °C, Al_2O_3 primarily formed $NH_4Al(SO_4)_2$, which decomposed into $Al_2(SO_4)_3$ at 600 °C and subsequently transformed into alumina (Al_2O_3) at 650 °C. At 500 °C, NiO primarily formed $NiSO_4$ and bunsenite (NiO); as the temperature increased to 650 °C, the diffraction peaks of $NiSO_4$ disappeared, resulting in complete transformation into bunsenite. At 500 °C, Cr_2O_3 formed $NH_4Cr(SO_4)_2$, $Cr_2(SO_4)_3$, and a small amount of Cr_2O_3. At 600 °C, $NH_4Cr(SO_4)_2$ almost completely decomposed, yielding $Cr_2(SO_4)_3$ as the main product, with the diffraction peaks of Cr_2O_3 becoming more pronounced. At 650 °C, $Cr_2(SO_4)_3$ was completely converted into Cr_2O_3. These findings elucidate that during the $(NH_4)_2SO_4$ calcination process of asbestos tailings, as the temperature increases, Fe, Al, Ni, and Cr ions progressively transform from soluble sulfate phases into insoluble oxides, which is a key factor contributing to

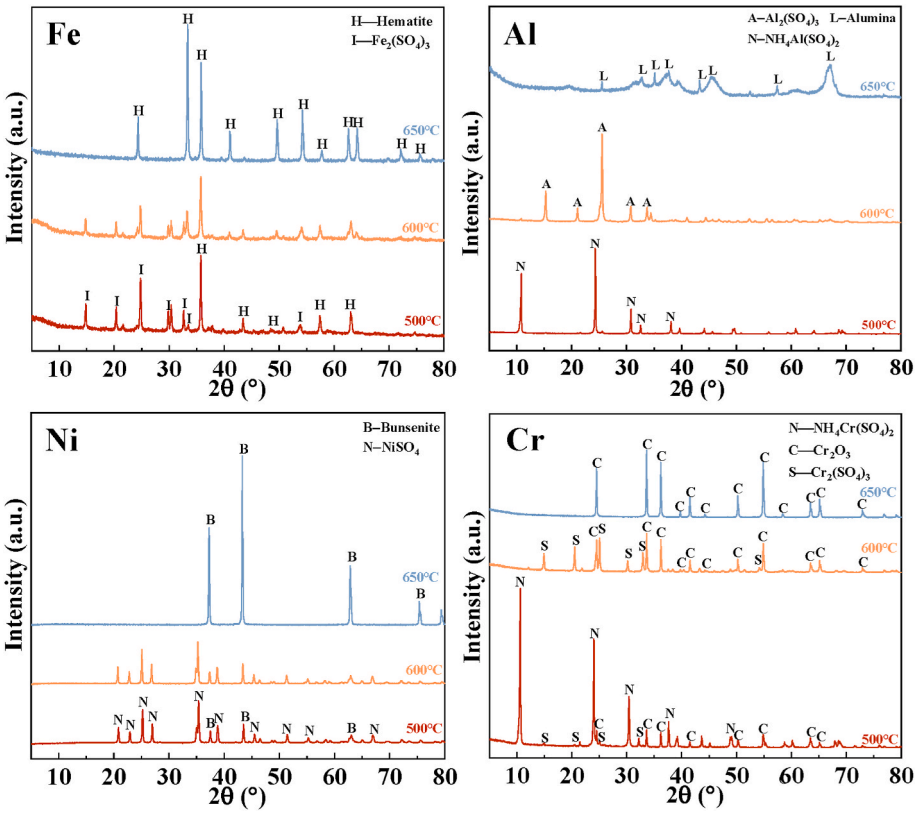

Fig. 8. XRD patterns of roasting slag at varying temperatures by $(NH_4)_2SO_4$ roasting with Fe_3O_4 (a), Al_2O_3 (b), NiO (c) and Cr_2O_3 (d).

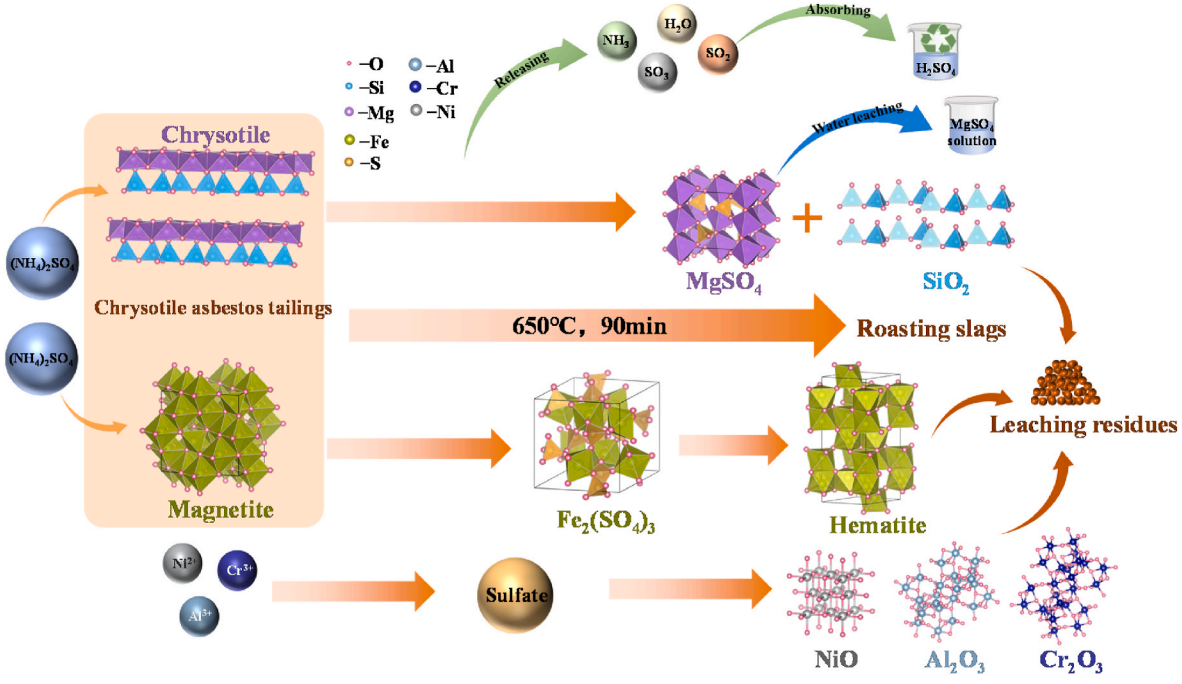

Fig. 9. Mechanism of selective separation of MgO from CAT via $(NH_4)_2SO_4$ roasting-leaching method.

the significant reduction in their leaching rates.

The mechanism for the selective extraction of Mg^{2+} from chrysotile asbestos tailings using the $(NH_4)_2SO_4$ roasting-leaching method is illustrated in Fig. 9. During the roasting process, chrysotile in CAT reacts with $(NH_4)_2SO_4$ or its decomposed product NH_4HSO_4 to form $MgSO_4$. Meanwhile, magnetite initially converted to $Fe_2(SO_4)_3$ in the presence of $(NH_4)_2SO_4$ or NH_4HSO_4. As the roasting temperature increases and the roasting time extends, $Fe_2(SO_4)_3$ transforms into insoluble hematite, releasing SO_2 and SO_3. Water leaching then selectively extracts Mg^{2+}, enriching iron in the leaching residues as hematite. Similarly, Al^{3+}, Cr^{3+}, and Ni^{2+} are initially converted to sulfates during the roasting process and ultimately decompose into oxides at high temperatures. The

NH_3, SO_2, and SO_3 released during roasting can be absorbed and recycled using dilute sulfuric acid solution.

3.5. Process evaluation

Building upon the aforementioned research, a sustainable process for utilizing chrysotile asbestos tailings has been developed, as illustrated in Fig. 10a. The $(NH_4)_2SO_4$ roasting method converts Mg^{2+} in CAT into soluble $MgSO_4$, which is selectively extracted via water leaching, leaving Fe^{2+}/Fe^{3+}, Al^{3+}, Cr^{3+}, and Ni^{2+} as oxides in the residue. The $MgSO_4$ solution can be further processed to produce high-purity magnesium carbonate and other magnesium-containing compounds (Ning et al., 2022). During the roasting process, NH_3 and small amounts of SO_2 are generated, both of which can be absorbed and recycled using a dilute sulfuric acid solution. For the processing of 1000 kg of chrysotile asbestos tailings, 1172 kg of $(NH_4)_2SO_4$ is required. The main components of the leachate residue include SiO_2, Fe_2O_3, along with minor amounts of MgO, Cr_2O_3, and NiO. Alkaline leaching facilitates the selective extraction of SiO_2 to generate a sodium metasilicate solution, which can then be employed in the production of white carbon black (Febriana et al., 2020). Additionally, the alkaline leaching residue can be directly used as an iron concentrate.

To investigate the environmental impact of the process above, a comprehensive life cycle assessment (LCA) was performed using the Gabi software. Given that the processes in stages S2, S3, and S4 are relatively mature and have been extensively documented, parameters from existing literature were directly utilized for the calculations (Table S1). Additionally, considering the hazardous nature of chrysotile tailings, they were treated as zero-emission raw materials in this analysis. The LCA analysis revealed that the carbon emission impact of the process, from highest to lowest, is as follows: S1 > S2 > S4 > S3 (Fig. 10b) to handle one ton of chrysotile tailings. Notably, the carbon emissions at the roasting process accounted for 82 % of the total of the S1 stage, indicating that it is the primary source of carbon emissions in the entire process. The standardized results across various impact categories further indicated that the process has significant impacts on global warming potential (GWP), abiotic depletion potential (ADP), and human toxicity potential (HTP) (Fig. 10c). Specifically, the high-energy-consuming roasting process is the main driver of global warming. Therefore, enhancing the energy efficiency of the roasting process, such as by using renewable energy sources like solar or wind power, could significantly reduce the overall carbon emissions of the process. Resource consumption is closely linked to the utilization of auxiliary materials. Improving the recovery and recycling efficiency of ammonium sulfate would help lower resource consumption. Human toxicity primarily originates from the crushing and grinding processes of chrysotile tailings. The use of enclosed ball mills or other enclosed grinding equipment in industry can greatly reduce this risk.

A comparison between the process proposed in this study and other methods for extracting Mg^{2+} from chrysotile asbestos tailings is presented in Table 3. This study proposes an $(NH_4)_2SO_4$ roasting-water leaching process for the extraction of Mg^{2+} from chrysotile asbestos tailings. Compared to acid leaching and conventional $(NH_4)_2SO_4$ roasting methods, this process is more efficient and environmentally friendly while effectively addressing the issue of co-leaching impurity metal ions. This method is not only applicable to the treatment of chrysotile asbestos tailings but can also be extended to the resource utilization of other magnesium-containing minerals, offering significant application potential. However, the transformation of chrysotile to forsterite at high temperatures reduces Mg^{2+} leaching efficiency, so future research will focus on inhibiting forsterite formation during roasting to enhance process efficiency.

4. Conclusions

(1) Under the conditions of an $(NH_4)_2SO_4$ to MgO in CAT molar ratio of 1.0, a roasting temperature of 650 °C, a roasting time of 90 min, a liquid-to-solid ratio of 8 mL/g, and a water leaching temperature of 30 °C, the leaching rate of Mg^{2+} reaches 84.18 %, with a purity of 98.87 % in the filtrate.

(2) During the roasting process of $(NH_4)_2SO_4$ roasting process, chrysotile in the tailings reacts with $(NH_4)_2SO_4$ or its decomposed form, NH_4HSO_4, resulting in the formation of $MgSO_4$. Magnetite reacts to form $Fe_2(SO_4)_3$, which further convert to hematite as the roasting temperature and time increase. Similarly, Al^{3+}, Cr^{3+}, and Ni^{2+} initially convert to soluble sulfates and subsequently

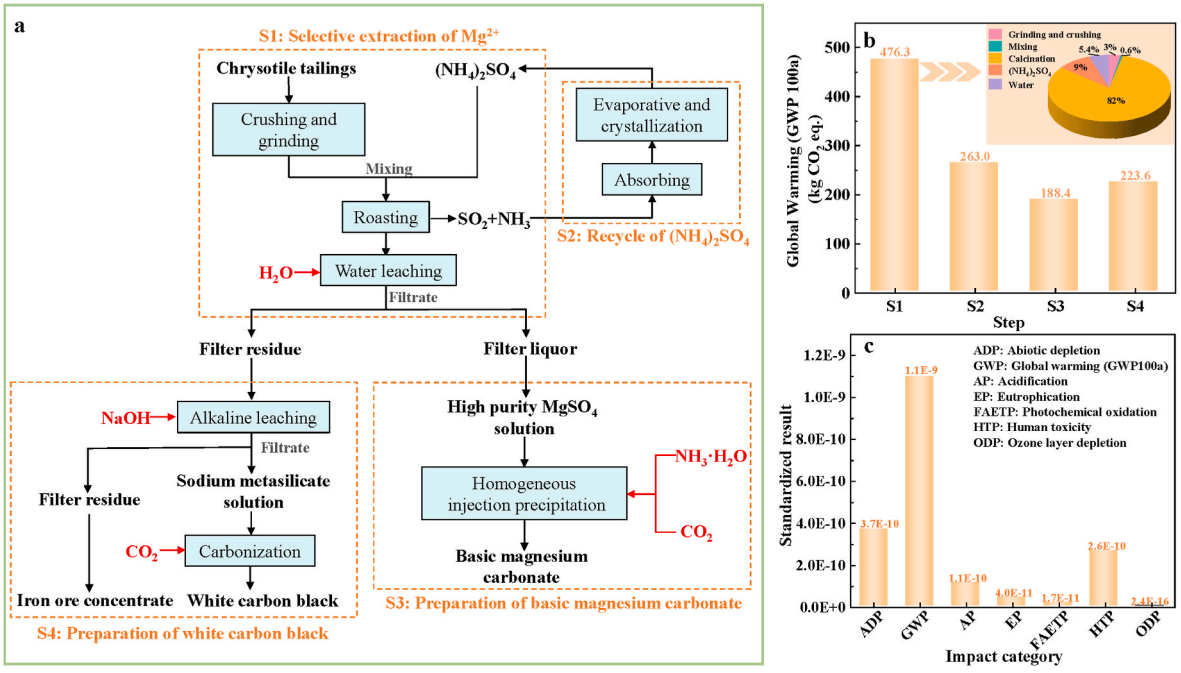

Fig. 10. Resource utilization process for chrysotile asbestos tailings (a); Carbon emissions of different process stages (b); Effects of processes on different environmental impact category (c).

Table 3
Comparison of methods for extracting Mg^{2+} from chrysotile asbestos tailings.

Roasting additive	Leaching solvent	Specific parameters	Leaching effect	Purification	References
None	Sulfuric acid	16.7 % sulfuric acid solution, leaching time: 10 min	Mg^{2+} leaching rate: 80 %–85 %	pH adjusted to 8 using NaOH	Sierra et al. (2018)
Ammonium sulfate	Water	Roasting temperature: 250 °C–550 °C, roasting time: 30 min–60 min	Maximum Mg^{2+} leaching rate: 66 %	pH adjusted to 9–10 using 25 % ammonia solution	Nduagu et al. (2013)
Ammonium sulfate or ammonium bisulfate	Water	Roasting temperature: 440 °C–480 °C, heating rate ≥40 °C/min, chrysotile/ammonium sulfate mass ratio:0.7	Maximum Mg^{2+} leaching rate: 58 %	Not mentioned	Nduagu et al. (2014)
None	Ammonium sulfate and ammonium bisulfate	Roasting temperature: 330 °C–350 °C, leaching temperature: 70 °C–90 °C, ammonium sulfate/ammonium bisulfate molar ratio: 1:1, HSO- 4/Mg^{2+} molar ratio: 3∼6	Mg^{2+} leaching rate: 75 %–80 %	Not mentioned	Erlund et al. (2016)
None	Sulfuric acid and fluorite	0.75 g fluorite, 3 mol/L sulfuric acid, leaching temperature: 80 °C, leaching time: 120 min	Maximum Mg^{2+} leaching rate: 93.69 %	Not mentioned	Peng et al. (2021)
Ammonium sulfate	Water	Chrysotile/ammonium sulfate mass ratio: 0.5–0.7, reaction temperature: 400 °C–440 °C, reaction time: 30 min–60 min	Mg^{2+} leaching rate: 64 %–66 %	Iron precipitated using ammonia solution	Nduagu et al. (2012)
None	Organic acids produced by aspergillus niger	Chrysotile suspension concentration: 1 %	Maximum leaching rates for Mg^{2+}, Fe^{2+}/Fe^{3+}, Co^{2+}, Ni^{2+}, and Mn^{4+}: 68 %, 20 %, 50 %, 16 %, and 67 %, respectively	Not mentioned	Dong et al. (2012)
Concentrated sulfuric acid	Water	Ore to acid ratio: 0.8:1, roasting temperature: 650 °C, roasting time: 120 min	Mg^{2+}, Ni^{2+}, and Fe^{2+}/Fe^{3+} leaching rates: 91.6 %, 88.7 %, 4.8 %, respectively	Not mentioned	Yang et al. (2022)
Ammonium sulfate	Water	Ammonium sulfate addition ratio ($(NH_4)_2SO_4$/MgO): 1.0, roasting temperature: 650 °C, roasting time: 90 min, liquid-to-solid ratio: 8 mL/g, water leaching temperature: 30 °C	Mg^{2+} leaching rate: 84.18 %, Fe^{2+}/Fe^{3+}, Al^{3+}, Cr^{3+}, Ni^{2+}, Ca^{2+} leaching rates: 0.04 %, 0.24 %, 0.09 %, 5.37 %, 53.61 %, respectively	No impurity removal steps are required, and the purity can reach 98.87 %	This study

decompose into insoluble oxides at high temperatures. The water leaching process enables the selective extraction of Mg^{2+}.

(3) LCA identified the roasting process as the main source of carbon emissions. Future sustainability improvements can be achieved by using clean energy sources such as solar or wind power and by enhancing the cycle efficiency of ammonium sulfate.

However, the process has limited effectiveness in extracting Mg^{2+} from asbestos tailings with high impurity mineral (such as talc) content and cannot effectively separate Ca^{2+}. Future research should focus on exploring the applicability of the process to different wastes and improving techniques for Ca^{2+} removal.

CRediT authorship contribution statement

Lingyan Chu: Writing – original draft, Software, Methodology, Investigation, Formal analysis, Conceptualization. **Hongjuan Sun:** Data curation, Funding acquisition, Writing – original draft. **Tongjiang Peng:** Investigation, Visualization. **Haichen Lu:** Resources, Supervision. **Maoting Li:** Software, Validation. **Yiqin Zhang:** Visualization, Writing – review & editing. **Liming Luo:** Funding acquisition, Project administration.

Declaration of competing interest

The authors declare that they have no known competing financial interests or personal relationships that could have appeared to influence the work reported in this paper.

Acknowledgment

This work was supported by the National Key Research and Development Program of China (2024YFC3907602); the Sichuan Science and Technology Program (2025ZNSFSC0437). The authors express their gratitude to Dr. Huan Gao from Chengdu University of Technology for the support in the field of life cycle assessment.

Appendix A. Supplementary data

Supplementary data to this article can be found online at https://doi.org/10.1016/j.jclepro.2025.145773.

Data availability

Data will be made available on request.

References

Alexander, G., Mercedes Maroto-Valer, M., Gafarova-Aksoy, P., 2007. Evaluation of reaction variables in the dissolution of serpentine for mineral carbonation. Fuel (Guildf.) 86, 273–281. https://doi.org/10.1016/j.fuel.2006.04.034.

Andersen, A.B.A., Henriksen, C., Wang, Q., Ravnsbæk, D.B., Hansen, L.P., Nielsen, U.G., 2021. Synthesis and Thermal degradation of $MAl_4(OH)_{12}SO_4{\cdot}3H_2O$ with M = Co^{2+}, Ni^{2+}, Cu^{2+}, and Zn^{2+}. Inorg. Chem. 60, 16700–16712. https://doi.org/10.1021/acs.inorgchem.1c02579.

Baigenzhenov, O.S., Kozlov, V.A., Luganov, V.A., Mishra, B., Shayahmetova, R.A., Aimbetova, I.O., 2015. Complex processing of wastes generated in chrysotile asbestos production. Miner. Process. Extr. Metall. Rev. 36, 242–248. https://doi.org/10.1080/08827508.2014.955610.

Cavallo, A., 2020. Environmental asbestos contamination in an abandoned chrysotile mining site: the example of val malenco (central alps, northern Italy). Episodes 43, 851–858. https://doi.org/10.18814/epiiugs/2020/0200s01.

Chen, J., Jak, E., Hayes, P.C., 2021. Investigation of the reduction roasting of saprolite ores in the caron process: microstructure evolution and phase transformations. Miner. Process. Extr. Metall. (IMM Trans. Sect. C) 130, 148–159. https://doi.org/10.1080/25726641.2019.1699361.

Deng, Z., Yang, F., Wei, C., Zhu, B., Zeng, P., Li, X., Li, C., Li, M., 2020. Transformation behavior of ferrous sulfate during hematite precipitation for iron removal. Trans. Nonferrous Metals Soc. China 30, 492–500. https://doi.org/10.1016/S1003-6326(20)65229-3.

Dong, F., Tan, Y., Yang, W., Zhang, W., Zhou, Y., 2012. Bioleaching of metals from tail-serpentine by Aspergillus Niger. In: Broekmans, M.A.T.M. (Ed.), Proceedings of the 10th International Congress for Applied Mineralogy (ICAM). Springer Berlin Heidelberg, Berlin, Heidelberg, pp. 145–152. https://doi.org/10.1007/978-3-642-27682-8_19.

Dong, F.Q., Zhou, Q., Peng, T.J., 2015. Utilization of serpentine resources in China. MSF 814, 583–589. https://doi.org/10.4028/www.scientific.net/MSF.814.583.

El-Sayed, D., Ismail, A.K., El-Hosiny, F.I., 2023. Magnesium chloride crystals with studying mechanism and leaching kinetics of serpentinite ore by hydrochloric acid. Trans. Indian Inst. Met. 76, 1439–1446. https://doi.org/10.1007/s12666-022-02852-7.

Erlund, R., Koivisto, E., Fagerholm, M., Zevenhoven, R., 2016. Extraction of magnesium from four Finnish magnesium silicate rocks for CO_2 Mineralisation—Part 2: aqueous

solution extraction. Hydrometallurgy (Amst.) 166, 229–236. https://doi.org/10.1016/j.hydromet.2016.07.004.
Febriana, E., Manurung, U.A.B., Prasetyo, A.B., Handayani, M., Muslih, E.Y., Nugroho, F., Sulistiyono, E., Firdiyono, F., 2020. Dissolution of quartz sand in sodium hydroxide solution for producing amorphous precipitated silica. IOP Conf. Ser. Mater. Sci. Eng. 858, 012047. https://doi.org/10.1088/1757-899X/858/1/012047.
Highfield, J., Lim, H., Fagerlund, J., Zevenhoven, R., 2012. Activation of serpentine for CO_2 mineralization by flux extraction of soluble magnesium salts using ammonium sulfate. RSC Adv. 2, 6535. https://doi.org/10.1039/c2ra01347a.
Hui, T., Sun, H.J., Peng, T.J., 2021. Preparation and characterization of cordierite-based ceramic foams with permeable property from asbestos tailings and coal fly ash. J. Alloys Compd. 885, 160967. https://doi.org/10.1016/j.jallcom.2021.160967.
Ju, J., Feng, Y., Li, H., Ma, R., Li, Y., Zhao, H., Wang, H., Jiang, S., 2024. An innovative method for the efficient and selective extraction of Co, Ni, Cu, and Mn from Oceanic cobalt-rich crusts by ammonium sulfate roasting: behavior, roasting kinetics and mechanism. Miner. Eng. 207, 108543. https://doi.org/10.1016/j.mineng.2023.108543.
Ju, J., Feng, Y., Li, H., Wu, R., Xue, Z., Ma, R., 2023a. High-efficiency and environment-friendly separation and recovery of manganese from braunite via the ammonium sulfate roasting-water leaching process: behavior and mechanism. Chemical Engineering Journal 466, 143218. https://doi.org/10.1016/j.cej.2023.143218.
Ju, J., Feng, Y., Li, H., Xu, C., Xue, Z., Wang, B., 2023b. Extraction of valuable metals from minerals and industrial solid wastes via the ammonium sulfate roasting process: a systematic review. Chemical Engineering Journal 457, 141197. https://doi.org/10.1016/j.cej.2022.141197.
Ju, J., Ma, R., Li, Y., Feng, Y., Li, H., Wang, H., Jiang, S., 2023c. An efficient and clean method for the selective extraction and recovery of manganese from pyrolusite using ammonium sulfate roasting-water leaching and carbonate precipitation. Miner. Eng. 203, 108356. https://doi.org/10.1016/j.mineng.2023.108356.
Kabombo, D., Azizi, D., Hébert, R., Larachi, F., 2021. Multistep concentration of lizardite/antigorite from chrysotile mine tailings – case of the carey mine site in east-broughton (québec). Int. J. Chem. React. Eng. 19, 483–498. https://doi.org/10.1515/ijcre-2020-0242.
Kaya, Ş., Topkaya, Y.A., 2011. High pressure acid leaching of a refractory lateritic nickel ore. Miner. Eng. 24, 1188–1197. https://doi.org/10.1016/j.mineng.2011.05.004.
Lacalamita, M., Ventruti, G., Della Ventura, G., Radica, F., Mauro, D., Schingaro, E., 2021. In situ high-temperature X-ray powder diffraction and infrared spectroscopic study of melanterite, $FeSO_4{\cdot}7H_2O$. Minerals 11, 392. https://doi.org/10.3390/min11040392.
Lente, G., Fábián, I., 2002. Kinetics and mechanism of the oxidation of sulfur(iv) by iron (iii) at metal ion excess. J. Chem. Soc., Dalton Trans. 778. https://doi.org/10.1039/b107263c.
Lévesque, A., Bélanger, N., Poder, T.G., Filotas, É., Dupras, J., 2020. From white to green gold: digging into public expectations and preferences for ecological restoration of asbestos mines in southeastern Quebec, Canada. Extr. Ind. Soc. 7, 1411–1423. https://doi.org/10.1016/j.exis.2020.10.006.
Li, C., Niu, J., Wang, X., Liang, X., Li, X., Lv, F., Yu, S., Yu, J., 2025. Direct fabrication of high-purity magnesium ingot using vacuum distillation technology. Separation and Purification Technology 366, 132835. https://doi.org/10.1016/j.seppur.2025.132835.
Li, J., Chen, Z., Shen, B., Xu, Z., Zhang, Y., 2017. The extraction of valuable metals and phase transformation and formation mechanism in roasting-water leaching process of laterite with ammonium sulfate. J. Clean. Prod. 140, 1148–1155. https://doi.org/10.1016/j.jclepro.2016.10.050.
Li, X., Ding, D., Xie, W., Zhang, Y., Kong, L., Li, M., Li, M., Deng, S., 2024. Risk assessment and source analysis of heavy metals in soil around an asbestos mine in an arid Plateau region, China. Sci. Rep. 14, 7552. https://doi.org/10.1038/s41598-024-58117-4.
Li, X., Hu, B., Liu, N., Liu, X., Liu, C., He, X., He, S., 2022. Extraction of alumina from high-alumina fly ash by ammonium sulfate: roasting kinetics and mechanism. RSC Adv. 12, 33229–33238. https://doi.org/10.1039/D2RA06658K.
Li, J., Li, Y., Duan, H., Guo, X., Zhai, Y., 2018. Experimental and kinetic study of magnesium extraction and leaching from laterite nickel ore by roasting with ammonium sulfate. Russ. J. Non-Ferrous Metals 59, 596–604. https://doi.org/10.3103/S1067821218060123.
Li, Y., Liu, H., Peng, B., Min, X., Hu, M., Peng, N., Yuang, Y., Lei, J., 2015. Study on separating of zinc and iron from zinc leaching residues by roasting with ammonium sulphate. Hydrometallurgy (Amst.) 158, 42–48. https://doi.org/10.1016/j.hydromet.2015.10.004.
Liu, W., Peng, X., Liu, W., Zhang, N., Wang, X., 2022. A cost-effective approach to recycle serpentine tailings: destruction of stable layered structure and solvent displacement crystallization. Int. J. Min. Sci. Technol. 32, 595–603. https://doi.org/10.1016/j.ijmst.2022.03.004.
Liu, X., Feng, Y., Li, H., Yang, Z., Cai, Z., 2012. Recovery of valuable metals from a low-grade nickel ore using an ammonium sulfate roasting-leaching process. Int. J. Miner. Metall. Mater. 19, 377–383. https://doi.org/10.1007/s12613-012-0567-5.
Liu, X., Ma, Y., Yan, W., He, M., Li, L., Sui, X., Peng, B., 2023. Identify key serpentines antigorite, lizardite and chrysotile with various compositions and crystallographic orientations using micro-Raman spectroscopy. Solid Earth Sciences 8, 295–304. https://doi.org/10.1016/j.sesci.2023.10.003.
Liu, Y., Ma, B., Lv, Y., Wang, C., Chen, Y., 2023. Thermodynamics analysis and response surface methodology to investigate decomposition behaviors for lepidolite sulfation products in presence of coal. Sci. Total Environ. 888, 164089. https://doi.org/10.1016/j.scitotenv.2023.164089.
Liu, Y., Zhang, X., Ma, W., Zhao, Q., Liang, Z., 2024. Research on the recycling of waste lithium battery electrode materials using ammonium sulfate roasting. Mater. Chem. Phys. 318, 129221. https://doi.org/10.1016/j.matchemphys.2024.129221.
Lu, Y., Duan, F., Zhu, Y., Wang, A., 2023. Sustainable utilization metal ions of acid leaching clay wastewater to fabricate adsorbents for high-efficient removing Congo red and methyl violet. Chem. Eng. Res. Des. 194, 854–868. https://doi.org/10.1016/j.cherd.2023.05.035.
Lu, Y., Yu, H., Zhu, Y., Mu, B., Wang, A., 2022. Recovering metal ions from oxalic acid leaching palygorskite-rich clay wastewater to fabricate layered mixed metal oxide/carbon composites for high-efficient removing Congo red. Chemosphere 290, 132543. https://doi.org/10.1016/j.chemosphere.2021.132543.
Lv, X., Cui, F., Ning, Z., Free, M.L., Zhai, Y., 2019. Mechanism and kinetics of ammonium sulfate roasting of boron-bearing iron tailings for enhanced metal extraction. Processes 7, 812. https://doi.org/10.3390/pr7110812.
Mu, W., Cui, F., Huang, Z., Zhai, Y., Xu, Q., Luo, S., 2018. Synchronous extraction of nickel and copper from a mixed oxide-sulfide nickel ore in a low-temperature roasting system. J. Clean. Prod. 177, 371–377. https://doi.org/10.1016/j.jclepro.2017.12.260.
Nduagu, E., Björklöf, T., Fagerlund, J., Wärnå, J., Geerlings, H., Zevenhoven, R., 2012. Production of magnesium hydroxide from magnesium silicate for the purpose of CO_2 mineralisation – part 1: application to Finnish serpentinite. Miner. Eng. 30, 75–86. https://doi.org/10.1016/j.mineng.2011.12.004.
Nduagu, E., Romão, I., Fagerlund, J., Zevenhoven, R., 2013. Performance assessment of producing $Mg(OH)_2$ for CO_2 mineral sequestration. Appl. Energy 106, 116–126. https://doi.org/10.1016/j.apenergy.2013.01.049.
Nduagu, E.I., Highfield, J., Chen, J., Zevenhoven, R., 2014. Mechanisms of serpentine–ammonium sulfate reactions: towards higher efficiencies in flux recovery and Mg extraction for CO_2 mineral sequestration. RSC Adv. 4, 64494–64505. https://doi.org/10.1039/C4RA08925A.
Ning, X., Wu, C., Chen, H., 2022. Preparation and characterization of novel 5Mg$(OH)_2{\cdot}MgSO_4{\cdot}7H_2O$ whiskers. Materials 15, 8018. https://doi.org/10.3390/ma15228018.
Peng, X., Liu, W., Liu, W., Zhao, L., Zhang, N., Gu, X., Zhou, S., 2021. Fluorite enhanced magnesium recovery from serpentine tailings: kinetics and reaction mechanisms. Hydrometallurgy (Amst.) 201, 105571. https://doi.org/10.1016/j.hydromet.2021.105571.
Raschman, P., Fedoročková, A., Sučik, G., 2013. Thermal activation of serpentine prior to acid leaching. Hydrometallurgy (Amst.) 139, 149–153. https://doi.org/10.1016/j.hydromet.2013.08.010.
Rashid, W., Alkadir, I., Jalhom, M., 2020. The solubility of phosphogypsum and recovery of heavy and radioactive elements. ETJ 38, 1470–1480. https://doi.org/10.30684/etj.v38i10A.907.
Sanna, A., Wang, X., Lacinska, A., Styles, M., Paulson, T., Maroto-Valer, M.M., 2013. Enhancing Mg extraction from lizardite-rich serpentine for CO_2 mineral sequestration. Miner. Eng. 49, 135–144. https://doi.org/10.1016/j.mineng.2013.05.018.
Sierra, C., Chouinard, S., Pasquier, L.C., Mercier, G., Blais, J.F., 2018. Feasibility study on the utilization of serpentine residues for $Mg(OH)_2$ production. Waste Biomass Valor 9, 1921–1933. https://doi.org/10.1007/s12649-017-9926-9.
Song, B., Liu, C., Zheng, S., Wang, T., Zhao, J., 2015. Study on the effect and mechanism of calcination of asbestos tailings mixed with ammonium sulfate. In: Dong, F. (Ed.), Proceedings of the 11th International Congress for Applied Mineralogy (ICAM), Springer Geochemistry/Mineralogy. Springer International Publishing, Cham, pp. 275–282. https://doi.org/10.1007/978-3-319-13948-7_28.
Song, B., Zhang, Y.R., Di, Y.H., Dai, R., Zheng, S.L., 2013. Study on calcination process of serpentine mixed with ammonium sulfate. AMM 320, 296–302. https://doi.org/10.4028/www.scientific.net/AMM.320.296.
Tagawa, H., 1984. Thermal decomposition temperatures of metal sulfates. Thermochim. Acta 80, 23–33. https://doi.org/10.1016/0040-6031(84)87181-6.
Tan, J., Ramakrishna, S., 2021. Applications of magnesium and its alloys: a review. Applied Sciences 11, 6861. https://doi.org/10.3390/app11156861.
Tan, Y., Zou, Z., Qu, J., Ren, J., Wu, C., Xu, Z., 2021. Mechanochemical conversion of chrysotile asbestos tailing into struvite for full elements utilization as citric-acid soluble fertilizer. J. Clean. Prod. 283, 124637. https://doi.org/10.1016/j.jclepro.2020.124637.
Thives, L.P., Ghisi, E., Thives Júnior, J.J., Vieira, A.S., 2022. Is asbestos still a problem in the world? A current review. J. Environ. Manag. 319, 115716. https://doi.org/10.1016/j.jenvman.2022.115716.
Tian, Z., Zhang, J., Zhang, Y., Fang, Y., Han, K., Li, Y., 2024. Thermochemical heat storage performance of Fe-doped MgO/$Mg(OH)_2$: experimental and DFT investigation. J. Energy Storage 86, 111388. https://doi.org/10.1016/j.est.2024.111388.
Wu, H., Li, J., Teng, W., Chen, Y., Liu, W., Ren, S., Yang, J., Liu, Q., 2023. One-step extraction of zinc and separation of iron from hazardous electric arc furnace dust via sulphating roasting-water leaching. J. Environ. Chem. Eng. 11, 111155. https://doi.org/10.1016/j.jece.2023.111155.
Xiao, Y., Chen, Y., Feng, Z., Huang, X., Huang, L., Long, Z., Cui, D., 2015. Leaching characteristics of ion-adsorption type rare earths ore with magnesium sulfate. Trans. Nonferrous Metals Soc. China 25, 3784–3790. https://doi.org/10.1016/S1003-6326(15)64022-5.
Xu, M., Kang, S., Jiang, F., Yan, X., Zhu, Z., Zhao, Q., Teng, Y., Wang, Y., 2021. A process of leaching recovery for cobalt and lithium from spent lithium-ion batteries by citric acid and salicylic acid. RSC Adv. 11, 27689–27700. https://doi.org/10.1039/D1RA04979H.

Yang, X., Gao, L., Wu, Y., Chen, Y., Tong, L., 2022. Extraction of magnesium and nickel from nickel-rich serpentine with sulfation roasting and water leaching. Metals 12, 318. https://doi.org/10.3390/met12020318.

Zhao, Z., Li, H., Wang, C., Xing, P., 2024. Transformation mechanism and selective leaching of nickel and cobalt from limonitic laterite ore using sulfation-roasting-leaching process. J. Clean. Prod. 445, 141327. https://doi.org/10.1016/j.jclepro.2024.141327.

Zheng, W., Sun, H., Peng, T., Zeng, L., Zhou, G., 2020. Pre-calcination of asbestos tailings and its recycling in refractory ceramics. Trans. Indian Ceram. Soc. 79, 106–111. https://doi.org/10.1080/0371750X.2020.1756412.

Zhou, L.S., Ming, D.Z., Li, Z.X., Li, H.P., 2013. The mechanism of thermal decomposition for ammonium sulfate and ammonium bisulfate via addition of ferric oxide. AMR (Adv. Magn. Reson.) 803, 68–71. https://doi.org/10.4028/www.scientific.net/AMR.803.68.